Iridium oxide (IV) nanoparticle-based lateral flow immunoassay

Daniel Quesada-González[a], Amadeo Sena-Torralba[a], Wiyogo Prio Wicaksono[a,b], Alfredo de la Escosura-Muñiz[a], Tribidasari A. Ivandini[b], Arben Merkoçi[a,c]*

[a]*Nanobioelectronics & Biosensors Group, Institut Català de Nanociència i Nanotecnologia (ICN2), CSIC and The Barcelona Institute of Science and Technology (BIST), Campus UAB, 08193, Bellaterra, Barcelona, Spain.*
[b]*Department of Chemistry, Faculty of Mathematics and Science, University of Indonesia, Kampus UI Depok, Jakarta 116424, Indonesia*
[c]*Institució Catalana de Recerca i Estudis Avançats (ICREA), P. Lluís Companys 23, 08010 Barcelona, Spain.*

Abstract:

Lateral flow biosensors are paper-based devices that allow the detection of different types of analytes with quickness, robustness and selectivity, without leaving behind paper sensors benefits as low-cost, recyclability and sustainability. Nanomaterials have been widely reported in lateral flow biosensors, offering new sensing strategies based on optical or electrical detection techniques. Looking for other advantageous nanomaterials, we propose for the first time the use of iridium oxide (IV) nanoparticles in lateral flow assays for the detection of human immunoglobulin as a model protein. These nanoparticles can be easily prepared and conjugated with biomarkers. Their dark blue colour gives a high contrast against the white background of the strips being in this way excellent labels.

*Corresponding author: arben.merkoci@icn2.cat

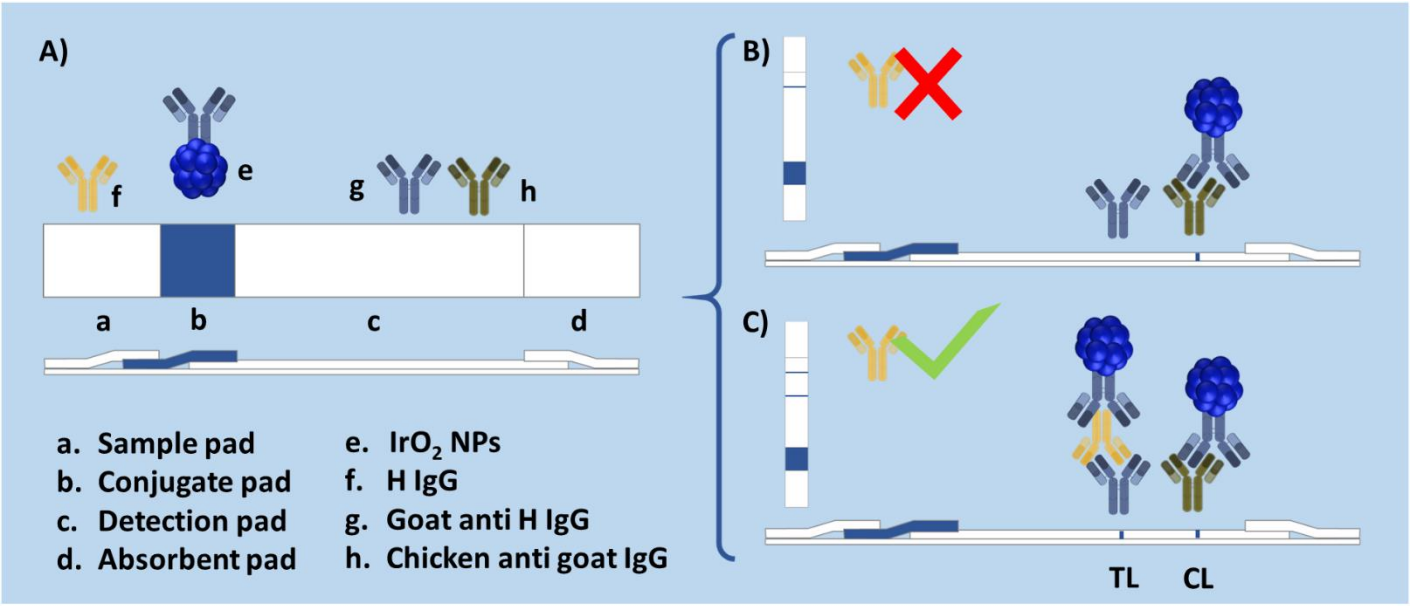

Figure 1. A) Schematic representation of a LF strip and its components a-h. B) Negative and C) positive performances.

1. Introduction

Lateral flow (LF) biosensors are paper-based simple platforms, presented on strip format, that permit easy and fast performance at low-cost without losing robustness, sensitivity or specificity (Parolo and Merkoçi, 2013; Posthuma-Trumpie *et al*., 2009; Quesada-González and Merkoçi, 2015; Sajid *et al*., 2015; Huang *et al*., 2016; López-Marzo and Merkoçi, 2016; Quesada-González and Merkoçi, 2018a). The development of LF biosensors could fulfill the demand of new point-of-care (PoC) devices, those which can be used at the time and place of care, even by the own patient (Li and Macdonald, 2016; Quesada-González and Merkoçi, 2018b), as well as environmental monitoring devices (Koedrith *et al*., 2015; Quesada-González *et al*., 2018c). Nowadays, more than half of the world population have a smartphone (Statista), thus it is an important tool to be considered as signal recorder in PoC biosensors (Ozan, 2014; Quesada-González and Merkoçi, 2016).

In this work we seek to improve the classical LF immunoassay with a new nanomaterial never applied before on this platform: iridium oxide (IV) nanoparticles (IrO_2 NPs). This nanomaterial exhibits a dark and intense blue color (Harriman and Thomas, 1987; Zhao *et al.* 2011; Xu *et al.*, 2015), demonstrated biocompatibility with antibodies (Rivas *et al.*, 2014a; Quesada-González *et al.*, 2019) and a wide specific surface to conjugate those (Finkelstein-Shapiro *et al.*, 2017).

The assay herein we present is based on the detection of human immunoglobulin (H IgG) as model protein (Parolo *et al*., 2013; Rivas *et al.*, 2014b) using IrO_2 NPs as tags, as shown on Fig. 1A. The operation principle of this LF assay follows the "direct method" or "standard design" (Quesada-González and Merkoçi, 2015), obtaining one colored line for negative samples (Fig. 1B) and two lines for positives (Fig. 1C).

2. Materials and methods

2.1. Materials

Cellulose membrane (CFSP001700), nitrocellulose membrane (HF180), glass fibber (GFCP00080000) and adhesive laminated cards (HF000MC100) were purchased from Millipore. Bovine serum albumin (BSA), sucrose, polyclonal goat anti-human IgG (I1886), Human IgG (I2511), phosphate buffer saline (PBS) tablets, sodium dodecyl sulfate (SDS), sodium tetraborate, orthoboric acid, drying pearls "orange" and Tween 20 were purchased from Sigma-Aldrich. Chicken anti-goat IgG (ab86245) was purchased from Abcam.

2.2. Instruments

Biospot Workstation from Biofluidix, Allegra 64 R Centrifuge, Biosan TS-100 Thermoshaker, Motorola "Moto Z" from Lenovo, hot plate Fisherbrand, Tecnai F20 TEM (FEI), SpectraMax iD3 Multi-Mode Microplate Reader.

2.3. Iridium oxide (IV) nanoparticles

2.3.1. Iridium oxide (IV) nanoparticles synthesis

IrO_2 NPs were produced according to Harriman and Thomas, 1987's work: 3.80 mM sodium citrate sesquihydrate (50 mg) and 1.24 mM K_2IrCl_6 (30 mg) were dissolved in 50 mL of MilliQ water and pH was adjusted to 7.5 by using 0.25 M NaOH. The brown solution

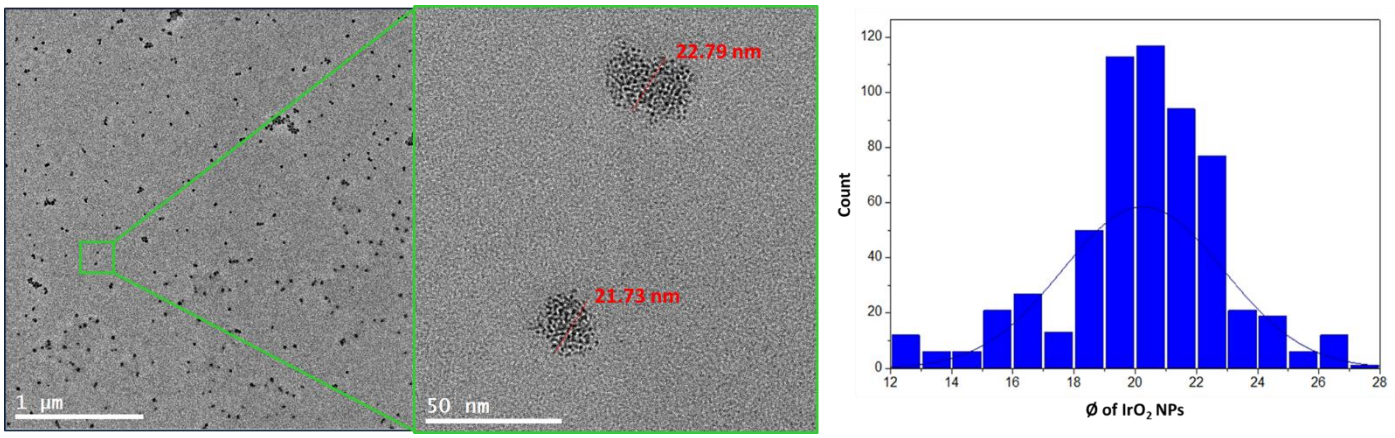

Figure 2. TEM images of IrO_2 NPS (left) and the corresponding histogram.

was taken to boiling point under vigorous stirring with a reflux until the color changed to light blue, keeping the solution heated 30 min more. The pH was checked after the solution was cooled down. If necessary, pH was readjusted to 7.5 and the 30 min boiling step was repeated until pH was steady. Then, the solution was boiled during 2 h in presence of bubbling oxygen. The obtained final solution was dark blue. Color changes during the synthesis can be observed on Fig. S1.

2.3.2. Iridium oxide (IV) nanoparticles conjugation

100 µL of anti-human IgG antibody produced in chicken (250 µg/mL) were mixed with 1.5 mL of IrO_2 NPs solution during 2h at 650 rpm and room temperature. The solution was then centrifuged at 35000 rcf and 4ºC during 2.5h. The solid was reconstituted immediately in 0.5 mL of borate buffer (2 mM, pH 7.4; made by mixing 2 mM sodium tetraborate with 2 mM orthoboric acid until the desired pH was achieved) containing 10% sucrose and 25% BSA.

2.3.3. Iridium oxide (IV) nanoparticles characterization

The reproducibility of IrO_2 NPs was checked after each synthesis by measuring their absorbance at 588 nm, were they exhibit a maximum absorbance peak wavelength. Fig. S2 shows the reproducibility of these measurements. In addition, IrO_2 NPs were characterized on transmission electron microscope (TEM) as shown on Fig. 2.

2.3.2. Iridium oxide (IV) nanoparticles stability evaluation

Gold nanoparticles (Au NPs), are often used in LF assays (Shyu *et al*., 2002; Oh *et al*., 2006; Parolo *et al*., 2013; Arun *et al.*, 2014; Singh *et al*., 2015; Karakus, 2015; Quesada-González *et al*., 2018c), but in presence of saline media these tend to aggregate (Pamies *et al.*, 2014; Christau *et al.*, 2017; Yang *et al.*, 2007). Instead, IrO_2 NPs are stable in saline media (Quesada-González *et al.*, 2019). To demonstrate it, the absorbance of Au NPs and IrO_2 NPs solutions was measured between 450 and 800 nm; then, a solution containing 10% NaCl was added and absorbance measured after 5 minutes (Fig. S3). Also, the stability in time of conjugated IrO_2 NPs was evaluated at different pH by measuring the absorbance spectra at pH 5, 7.4 and 8 during 5 weeks (Fig. S4). We chose buffered media commonly used on antibody assays: MES (pH 5), BB (pH 7.4) and Tris-HCl (pH 8). During this period of time, the solutions were kept at room temperature protected from light.

2.4. Lateral flow strips preparation

LF strips are formed by 4 different pads assembled on a laminated card: sample, conjugate, detection and sample pads.

Both sample and absorbent pads consist of cellulose membrane. Sample pad was made by dipping the membrane on 10 mM PBS solution at pH 7.4 containing 5% BSA and 0.05% Tween 20, then leaving it to dry during 2h at 37ºC. In the case of the absorbent pad treatments were not necessary. Sample and absorbent pad are placed on the bottom and the upper parts of the LF strip respectively, as illustrated on Fig. 1A(a,d).

Conjugate pad consists of glass fiber storing IrO_2 NPs conjugated with antibody. The reconstituted solution of IrO_2 and antibody (point 2.3.2) was carefully dispensed by drop-casting over the glass fiber and it was vacuum dried during 3 h. After this time it was stored overnight at room temperature in a hermetic box containing dry pearls. Conjugate pad is placed between detection and sample pads (Fig. 1A(b)).

Detection pad consists of nitrocellulose membrane and contains test (TL) and control (CL) lines, anti-human IgG and anti-goat IgG antibodies respectively. Both antibodies were dispensed using a Biospot Workstation with a dispensing rate of 0.05 µL/mm. After drying the membrane during 2h at 37ºC it was blocked by dispersing on it, using a spray, a 10 mM PBS solution at pH 7.4 containing 5% BSA. After 5 min the membrane was introduced into washing solution (PBS 2 mM at pH 7.4 with 0.05 % SDS) and shaken vigorously twice during 15 min. Membrane was finally dried during 2h at 37ºC. Detection pad is placed between absorbent and detection pads (Fig. 1A(c)).

Once the strips were assembled, LF strips were cut with a width of 6 mm.

2.5. Lateral flow immunoassay

Serial dilutions of H IgG were made in PBS (0.01 M, pH 7.4). The same buffer was used as blank. 200 µL of each solution, by triplicate, were dispensed on the sample pad of the LF strips and after 10 min the detection pads were photographed with a Samsung S9 mobile phone camera (Ozcan, 2014; Quesada-González and Merkoçi, 2016). In order to keep constant the distance between the mobile phone camera and the strips (60 mm) a simple support was 3D-printed (Fig. S5) with a Sigma BCN-3D machine. Environmental light was controlled by performing the photographs in a windows-free room. The images were later measured with ImageJ software (Adhikari *et al.*, 2015; Álvarez-Diduk *et al.*, 2016; Kühnemund *et al.*, 2017; Roda *et al.*, 2014). TL were measured in grayscale obtaining a value from 0 to 255 (pure black and pure white, respectively); that value was normalized by applying the formula:

$$V_n = (1/V_o - 1/V_{low}) / (1/V_{high})$$

Where V_n is the normalized value (from 0 to 1; being 0 the signal corresponding to the less colored LF strip and 1 the most colored one), V_o is the measured value from the LF strip (from 0 to 255), V_{low} the whitest value (closest number to 255 among all the LF strips) and V_{high} the blackest (closest number to 0 among all LF strips).

3. Results and discussion

3.1. Iridium oxide nanoparticles stability and characterization

On Fig. S2 it can be observed the corresponding spectra of IrO_2 NPs which exhibit a maximum absorbance peak wavelength at 588 nm (synthesis was reproduced in three different days). IrO_2 NPs stability in saline media was compared against Au NPs; as seen on Fig. S3, IrO_2 NPs are not agglomerated in presence of common salt. Stability in time of IrO_2 NPs at different pH was studied too, during 5 weeks (Fig. S4). They were shown to be stable at pH 5 and 7.4 (pH at which is prepared the conjugate pad), but not at alkaline pH (the blue colour of the solution is, even at naked eye, clearly different; it can also be appreciated during the synthesis of the nanoparticles when the pH is not well adjusted to 7.5 and goes by long adding NaOH).

Fig. 2 shows TEM images of IrO_2 NPs and the corresponding histogram from which the obtained nanoparticle average diameter was 20 ± 2 nm.

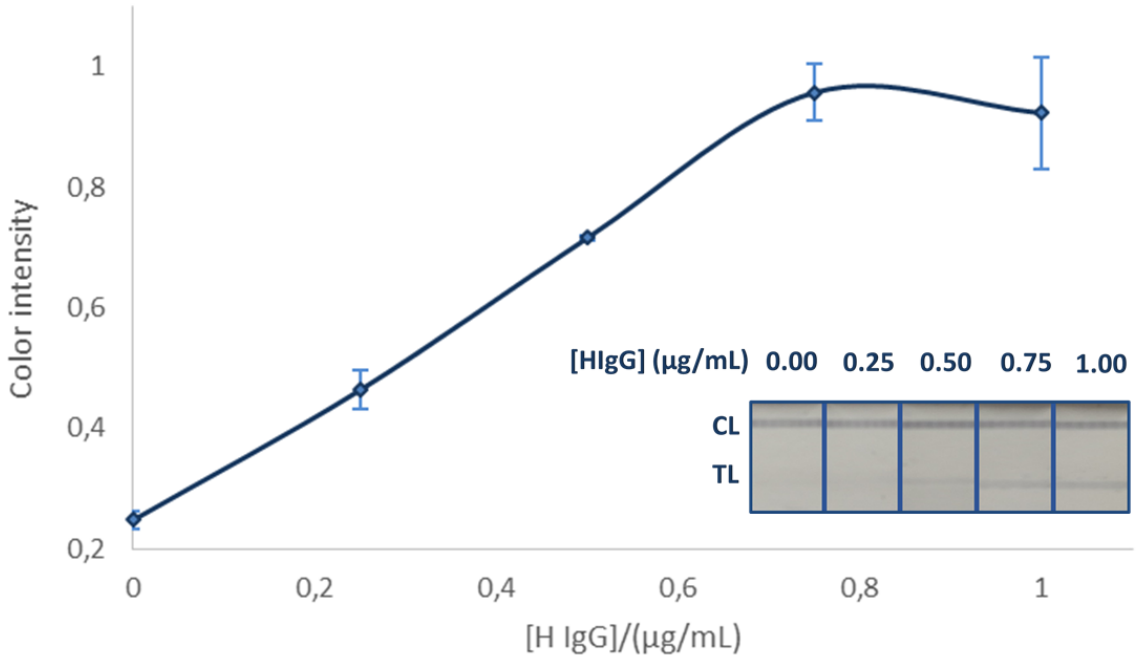

Figure 3. Optical response of LF strips to the concentration of H IgG. Inset of LF detection pads.

3.2. Lateral flow immunoassay

H IgG was diluted to different concentrations: 0.25, 0.50, 0.75 and 1.00 μg/mL. The solutions and blank sample were applied on LF strips. On Fig. 3 it is illustrated the measured intensities for each concentration and the images taken from different detection pads. At a concentration of H IgG over 0.75 μg/mL it is observed how the intensity is saturated; this effect is due an excess of analyte that is captured by all the antibodies linked to IrO_2 and nitrocellulose TL, impeding the stopping of more IrO_2 NPs on that area. Thus, the working range was defined between 0 and 0.75 μg/mL and represented by the equation:

color intensity = 0.95 [H IgG](μg/mL) + 0.24

The equation has an r value of 0.999. The method shows a reproducibility (RSD) of 3 % (n=3) for a H IgG concentration of 0.25 μg/mL. A limit of detection (LOD) (calculated from the calibration equation by substituting the "color intensity" value by the average signal of blank, 0.25 μg/mL, plus three times its standard deviation, 0.02 μg/mL) of 0.07 μg/mL is estimated.

As said before, Au NPs are commonly used on LF assays, thus our IrO_2 NPs LF test was compared with a Au NPs LF test repeated under the same conditions and with the same reagents and antibodies (Fig. S6). Au NPs were synthetized following Turkevich *et al.* (1951) method. Comparing both assays, IrO_2 NPs exhibit a higher intensity (2-fold at 1.00 μg/mL) when signal is captured by a smartphone. The dark blue color of IrO_2 NPs against the red color of Au NPs has a greater contrast in comparison with the white background of LF strips, which is an advantage for the adaptation to smartphone measurements, leaving aside tailor-made colorimetric readers (e.g. for AuNPs a colorimetric reader focused on 520 nm wavelength should be required).

4. Conclusion

We have demonstrated for the first time that IrO_2 NPs can be used on LF tests for the detection of a model protein, H IgG. Our test has exhibited good LOD (0.07 μg/mL) and sensitivity (twice the sensitivity of the classical Au NPs LF test) with a smartphone as recording tool, which makes our system an interesting tool in PoC diagnostics.

In future work, IrO_2 NPs could lead to the integration of other detection techniques on LF strips (Quesada-González and Merkoçi, 2015) as they are electrochemical measurements. It would be possible since IrO_2 NPs have demonstrated interesting electrocatalytical properties against water oxidation reaction even in buffer medium (Rivas *et al.*, 2014a, 2015; Mayorga-Martinez *et al.*, 2014, 2015; Kurbanoglu *et al.*, 2017); it would be an advantage in comparison to the currently reported electrochemical LF assays in which the strips need to be treated with acid solutions in order to perform the measurements (Inoue *et al.*, 2007; Wicaksono and Putri, 2014), thus adding extra steps to the system and damaging the strip.

Acknowledgments

We acknowledge support from MINECO (Spain) MAT2017-87202-P and project PCIN-2016-066 (program Euronanomed 2). This work is also funded by the CERCA Programme / Generalitat de Catalunya. ICN2 is supported by the Severo Ochoa program from Spanish MINECO (Grant No. SEV-2013-0295). Daniel Quesada-González also acknowledges Autonomous University of Barcelona (UAB) for the possibility of performing this work inside the framework of Chemistry PhD Programme.

References

Adhikari, M., Strych, U., Kim, J., Goux, H., Dhamane, S., Poongavanam, M. V., Hagström, A. E. V., Kourentzi, K., Conrad, J. C., Willson, R. C., 2015. Anal. Chem. 87 (23), 11660–11665.

Álvarez-Diduk, R., Orozco, J., Merkoçi, A., 2017. Sci. Rep. 7, 976.

Arun, T. R., Rana, R., Singh, P., Choudhuri, P., Singh, V. P. Thomas, P., Rekha, V., Nehra, K., Usharani, J., Dhama, K., 2014. AJAVA 9 (7), 405-413.

Christau, S., Moeller, T., Genzer, J., Koehler, Ralf, 2017. Macromolecules 50 (18), 7333-7343.

Finkelstein-Shapiro, D., Fournier, M., Méndez-Hernández, D. D., Guo, C., Calatayud, M., Moore, T. A., Moore, A. L., Gust, D., Yarger, J. L., 2017. Phys. Chem. Chem. Phys. 19, 16151-16158.

Harriman, A., Thomas, J. M., 1987. New J. Chem. 11, 757.

Huang, X., Aguilar, Z. P., Xu, H., Lai, W., Xiong, Y., 2016. Biosens. Bioelectron. 75, 166-180.

Inoue, K., Ferrante, P., Hirano, Y., Yasukawa, T., Shiku, H., Matsue, T., 2007. Talanta 73, 886–892.

Karakus, C., 2015. J. Immunoassay Immunochem. 36, 324–333.

Koedrith, P., Thasiphu, T., Weon, J. I., Boonprasert, R., Tuitemwong, K., Tuitemwong, P., 2015. Sci. World J. 2015, 510982.

Kühnemund, M., Wei, Q., Darai, E., Wang, Y., Hernández-Neuta, I., Yang, Z., Tseng, D., Ahlford, A., Mathot, L., Sjöblom, T., Ozcan, A., Nilsson, M., 2017. Nat. Commun. 8, 13913.

Kurbanoglu, S., Rivas, L., Ozkan, S. A., Merkoçi, A., 2017. Biosens. Bioelectron. 88, 122-129.

Li, J., Macdonald, J., 2016. Biosens. Bioelectron. 83, 177-192.

López-Marzo, A. M., Merkoçi, A., 2016. Lab Chip, 16, 3150-3176.

Mayorga-Martinez, C. C., Pino, F., Kurbanoglu, S., Rivas, L., Ozkan, S. A., Merkoçi, A., 2014. J. Mater. Chem. B 2, 2233-2239.

Oh, J. S., Ha, G. W., Cho, Y. S., Kim, M. J., An, D. J., Hwang, K. K., Lim, Y. K., Park, B. K., Kang, B. K., Song, D. S., 2006. Clin. Vaccine Immunol. 13(4), 520–524.

Ozcan, A., 2014. Lab Chip 14, 3187-3194.

Pamies, R., Hernández Cifre, J. G., Fernández Espín, V., Collado-González, M., Díaz Baños, F. G., García de la Torre, J., 2014. J. Nanopart. Res. 16, 2376.

Parolo, C., Merkoçi, A., 2013. Chem. Soc. Rev. 42, 450–457.

Parolo, C., Medina-Sánchez, M, de la Escosura-Muñiz, A., Merkoçi, A., 2013. Lab Chip 13, 386-390.

Posthuma-Trumpie, G. A., Korf, J., van Amerongen, A., 2009. Anal. Bioanal. Chem. 393 (2), 569-582.

Quesada-González, D., Merkoçi, A., 2015. Biosens. Bioelectron. 73, 47-63.
Quesada-González, D., Merkoçi, A., 2016. Biosens. Bioelectron. 92, 549–562.
Quesada-González, D., Merkoçi, A., 2018a. Actualidad Analítica 63, 43-46.
Quesada-González, D., Merkoçi, A., 2018b. Chem. Soc. Rev., 47, 4697-4709.
Quesada-González, D., Jairo, G. A., Blake II, R.C., Blake, D. A., Merkoçi, A. 2018c. Sci. Rep. 8, 16157.
Quesada-González, D., Baiocco, A., Martos, A. A., de la Escosura-Muñiz, A., Palleschi, G., Merkoçi, A., 2019. Biosens. Bioelectron., 127, 150-154.
Rivas, L., de la Escosura-Muñiz, A., Pons, J., Merkoçi, A., 2014a. Electroanal. 26, 1287-1294.
Rivas, L., Medina, M., de la Escosura-Muñiz, A., Merkoçi, A., 2014b. Lab Chip 14, 4406-4414.
Rivas, L., Mayorga-Martinez, C. C., Quesada-González, D., Zamora, A., de la Escosura-Muñiz, A., Merkoçi, A., 2015. Anal. Chem. 87 (10), 5167–5172.
Roda, A., Michelini, E., Cevenini, L., Calabria, D., Calabretta, M. M., Simoni, P., 2014. Anal. Chem. 86, 7299−7304.
Sajid, M., Kawde, A. N., Daud, M., 2015. J. Saudi Chem. Soc. 19 (6), 689-705.
Shyu, R. H., Shyu, H. F., Liu, H. W., Tang, S. S., 2002. Toxicon 40, 255–258.
Singh, J., Sharma, S., Nara, S., 2015. Food Chem. 170, 470-483.
Statista (mobile phone users in the world). Webpage: https://www.statista.com/statistics/274774/forecast-of-mobile-phone-users-worldwide/ (last accessed 2018/06/29).
Turkevich, J., Stevenson, P. C., Hillier, J., 1951. Discuss. Faraday Soc. 11, 55–75.
Wicaksono, W. P., Putri, A. P., 2014. Applied Mech. Mater. 490, 1624-1628.
Xu, D., Diao, P., Jin, T., Wu, Q., Liu, X., Guo, X., Gong, H., Li, F., Xiang, M., Ronghai, Y., 2015. ACS Appl. Mater. Interfaces 7 (30), 16738–16749.
Yang, Y., Matsubara, S., Nogami, M., Shi, J., 2007. Mater. Sci. Eng. B 140 (3), 172-176.
Zhao, Y., Hernandez-Pagan, E. A., Vargas-Barbosa, N. M., Dysart, J. L., Mallouk, T. E., 2011. J. Phys. Chem. Lett. 2 (5), 402–406.